

RESEARCH ARTICLE

Constraining the size of the carrier of the $\lambda 5797.1$ diffuse interstellar band

Jane Huang and Takeshi Oka

Department of Chemistry and Department of Astronomy and Astrophysics,
the Enrico Fermi Institute, University of Chicago, Chicago, Illinois, USA 60637

(Received 00 Month 200x; final version received 00 Month 200x)

The diffuse interstellar band (DIB) at 5797.1 \AA is simulated based on three premises: (1) The carrier of the DIB is polar as concluded by T. Oka et al. from the anomalous spectrum toward Herschel 36. (2) The sharp central feature observed by P. J. Sarre's group is the Q -branch of a parallel band of a prolate top. (3) The radiative temperature of the environment is $T_r = 2.73 \text{ K}$.

A ${}^2\Pi \leftarrow {}^2\Pi$ transition of a linear radical is simulated. Results depend on 10 parameters, with the rotational constant B being the most critical. Comparisons of calculated spectra with observed data constrain B , which in turn constrains the number of heavy atoms to $5 \leq n \leq 7$. Upper limits based on the Her 36 spectrum and lower limits based on stability against photodissociation are also discussed. The latter is based on the assumption that the DIB molecules are produced top-down from the breakdown of dust rather than bottom-up by chemical reactions.

A difficulty with this limit is that J. P. Maier's laboratory has observed many molecules within this size range, some of which have been tested astronomically. Candidates are discussed in light of many prolate tops observed by the P. Thaddeus and M. C. McCarthy microwave group.

Keywords: Diffuse interstellar bands; spectral simulation; carbon chain molecules; the diffuse interstellar medium

1. Introduction

A long-standing question in astronomical spectroscopy has been the identity of the carriers of the diffuse interstellar bands (DIBs). DIBs are broad absorption features, primarily in the visible region, that have been observed in the spectra of numerous stars [1, 2]. After the incidental observation of the strongest DIB at 4430 \AA (henceforth referred to as the $\lambda 4430$ DIB) by Annie Jump Cannon in the early years of stellar spectroscopy [3–5] and reports of the $\lambda\lambda 5780$ and 5797 DIBs by Mary Heger in 1922 [6, 7], Paul W. Merrill demonstrated in the 1930s that these spectral features arose due to intervening interstellar material [8, 9]. Laboratory spectroscopy and computational modeling have led to a diverse set of hypotheses for the origins of DIBs. Douglas argued for the consideration of long-chain carbon molecules based on the recently discovered cyano-polyacetylene [10] and the Douglas effect [11] as a broadening mechanism [12]. On the other hand, van der Zwet and Allamandola proposed polycyclic aromatic hydrocarbons (PAHs), based on their stability as well as their likelihood of forming free radicals that could

Current affiliation: Harvard-Smithsonian Center for Astrophysics, 60 Garden St., Cambridge, MA 02138
Corresponding author. e-mail: t-oka@uchicago.edu

absorb in the visible region [13]. A similar proposal by Léger and d’Hendecourt [14] was published back to back with [13].

Identifying specific DIB carriers would provide greater insight into the nature of the interstellar medium (ISM). If the carriers were known, the variations in DIB profiles along different lines of sight could be used to infer physical conditions [15]. Furthermore, DIBs have been detected in several moderate-redshift galaxies, which has helped to constrain how long ago their carriers first appeared and may provide information about the origins of organic compounds in the universe [16].

Among the 400 or so DIBs observed thus far [17, 18], the $\lambda\lambda 5780.5$, 5797.1 , 6196.0 , 6379.3 , and 6613.6 DIBs have been investigated in particular detail, both observationally and theoretically. The sharpness of these DIBs and substructures in some of these bands provide evidence that these DIBs are due to electronic transitions of gas-phase molecules [19–21]. High-resolution spectra of these bands has facilitated rotational contour fittings of DIB profiles, thereby enabling plausible sizes and geometries of carrier molecules to be assessed [21–25]. In this paper we attempt to simulate the observed profile of $\lambda 5797.1$, which has distinctive features that we believe are the most revealing of the properties of its carrier.

A remarkable recent development in DIBs studies has been the discovery of the special sightline toward the star Herschel 36 by York’s team in 2013, Dahlstrom et al. [26]. Unlike the more than 200 stars previously observed, this sightline shows rotationally excited CH^+ and CH , revealing the high radiative temperature, T_r , of the environment. The effect of high T_r is even more spectacular in DIBs; the $\lambda\lambda 5780.5$, 5797.1 , and 6613.6 DIBs show pronounced Extended Tails toward Red (ETR), while the $\lambda\lambda 5849.8$, 6196.0 , and 6379.3 DIBs are not much affected. They argued that the rotationally excited CH^+ and CH lines are due to far-infrared pumping by the nearby hot infrared source Her 36 SE discovered by Goto et al. [27], which is only $0.''25$ away from Her 36. Oka et al. [28] proposed that the ETRs are produced due to radiative pumping of the high rotational levels of polar carriers of the DIBs. This has introduced a new way to classify DIBs: (1) those that have polar molecule carriers, which are sensitive to T_r , and (2) those with non-polar carriers, which are insensitive to variations in T_r . Based on simulations of spectra of large linear molecules in which the rotational distribution was calculated by taking the radiative and collisional effects into account simultaneously, Oka et al. concluded that the carriers of the $\lambda\lambda 5780.5$, 5797.1 , and 6613.6 DIBs are polar molecules and that the ETRs are produced by a decrease in the rotational constant upon electronic excitation.

In this paper, we use Oka et al.’s model for the rotational distribution of the carrier to simulate the $\lambda 5797.1$ DIB. Earlier DIB modeling generally assumed a thermal Boltzmannian rotational distribution with a relatively high temperature, such as $T = 50$ K by Danks and Lambert [19] and by Ehrenfreund and Foing [22], $T = 8.9 - 101.3$ K by Kerr et al. [23], $T = 30 - 100$ K by Schulz et al. [24], $T = 10 - 100$ K by Walker et al. [21], and $T = 21.0 - 25.5$ K by Cami et al. [25]. This may give a reasonable approximation if the molecule is non-polar and the rotational distribution is governed by collisions. However, for polar molecules such as the predicted carrier type for the $\lambda 5797.1$ DIB, radiative effects dominate. Spontaneous emission and low collision rates make the excitation temperature of the rotational distribution close to the cosmic microwave background blackbody temperature $T = 2.73$ K [29]. This reduces the width of a DIB and allows us to constrain the size of the carrier with higher accuracy. So far, Cordiner and Sarre’s calculation of the $\lambda 8037$ DIB with CH_2CN^- as the carrier seems to be the only one in which $T_{ex} = T_r = 2.7$ K is used [30]. Cossart-Magos and Leach [31] and Edwards and Leach [32] used thermal distributions with $T_{ex} = 3$ K, although their

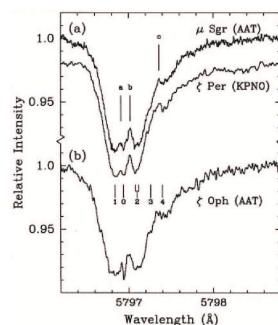


Figure 1. Spectra (resolving power of 600,000 at AAT and 300,000 at KPNO) of the $\lambda 5797.1$ DIB, originally published as Figure 2 in Kerr et al. [33]. Reprinted with permission of the main author (P. J. Sarre) and The Astrophysical Journal.

studies were on non-polar molecules.

2. Methods

2.1. The $\lambda 5797.1$ DIB

The substructures of the $\lambda 5797.1$ DIB were first studied at very high resolutions by Sarre’s group in the spectra of the stars μ Sgr, ζ Per, and ζ Oph [20, 33]. Figure 1 shows Kerr et al.’s spectra of the $\lambda 5797.1$ band for three lines of sight, observed either at the Anglo-Australian Telescope (AAT) at a resolving power of 600,000 or at Kitt Peak National Observatory at a resolving power of 300,000 [33]. As seen in all three lines of sight, the $\lambda 5797.1$ DIB shows a narrow spectral feature at its center, with two peaks on either side that are wider but at a similar depth. On the redward side of these three peaks, there is a shallow bump in the spectrum [33]. Later high-resolution studies of the $\lambda 5797.1$ DIB along several other lines of sight also consistently identified similar spectral features [34, 35].

The characteristic three features of the $\lambda 5797.1$ DIB, unique among known DIBs, are most naturally ascribed to the R -, Q -, and P -branches of a fairly simple molecule. The sharp and weak central feature suggests a Q -branch of a parallel transition, since a perpendicular transition would feature a stronger and broader Q -branch reminiscent of the central peak of the $\lambda 6613.6$ DIB. The carrier must be a prolate top, because otherwise the Q -branch would be stronger (see, for example, Cossart-Magos and Leach’s rotational contour simulations of PAHs as carriers [31]). For the Q -branch to appear, the carrier of the $\lambda 5797.1$ DIB should be either a linear molecule with non-zero orbital angular momentum Λ , or an asymmetric or symmetric rotor with a large A rotational constant, such as carbene with C_{2v} symmetry or methyl polyynes with C_{3v} symmetry. In this paper, we simulate the $\lambda 5797.1$ DIB as a ${}^2\Pi \leftarrow {}^2\Pi$ (parallel) transition of a linear molecule. Linear molecules with Δ ground states (i.e., $\Lambda = 2$) or with higher Λ are rare. The C_{2v} and C_{3v} molecules are not modeled in this paper, but the constraints on the rotational constant B and hence the size of the molecule should apply similarly. During the process of simulation, we found that modeling linear molecules was advantageous in that an additional parameter is made available by including a large spin-orbit interaction that changes upon electronic excitation.

Oka et al. [28] concluded that the ETRs for the $\lambda\lambda 5780.5$, 5797.1 , and 6613.6 DIBs observed toward Herschel 36 are caused by bond lengthening and hence a decrease of the rotational constant B upon excitation of the electronic state. For such a transition, vibronic bands involving stretching vibrations may have large Franck-Condon factors. Therefore, the $\lambda 5797.1$ DIB is likely accompa-

nied by fairly strong vibronic progressions. About 60 DIBs have been reported within 1000 cm^{-1} to the blue of the $\lambda 5797.1$ DIB toward both HD 204827 [17] and HD 183143 [18]. Identifying which of these many candidates are vibronic satellites of the $\lambda 5797.1$ DIB requires careful studies of correlations [36], progressions [37], and spectroscopy. Further work in this area will be attempted as a separate project in future publications.

2.2. Calculating rotational distributions

The population distribution of rotational levels for a polar linear molecule in this work was calculated using Oka et al.'s approach for modeling the Her 36 DIBs [28]. Accounting for both radiation and collisions, the relationship between the populations of the rotational levels in the $J \rightarrow J-1$ and $J \leftarrow J-1$ transitions is determined by the principle of detailed balancing [28]

$$n(J)(A^J + B_{J-1}^{\downarrow}\rho + C_{J-1}^{\downarrow}) = n(J-1)(B_{J-1}^{\uparrow}\rho + C_{J-1}^{\uparrow}), \quad (1)$$

where A^J is the Einstein coefficient for spontaneous emission, B_{J-1}^{\downarrow} and B_{J-1}^{\uparrow} are the Einstein coefficients for stimulated emission $J \rightarrow J-1$ and absorption $J \leftarrow J-1$, respectively, ρ is Planck's spectral energy density, and C_{J-1}^{\downarrow} and C_{J-1}^{\uparrow} are the collision rates.

From Equation (1), the following expression for number density was obtained by Oka et al. [28][38]

$$n(J) = n(0) \prod_{m=1}^J \frac{\alpha B^3 \mu^2 \frac{m^4}{2m-1} \frac{1}{\exp(2hBm/kT_r)-1} + C \sqrt{\frac{2m+1}{2m-1}} \exp\left(\frac{-hBm}{kT_k}\right)}{\alpha B^3 \mu^2 \frac{m^4}{2m+1} \left(1 + \frac{1}{\exp(2hBm/kT_r)-1}\right) + C \sqrt{\frac{2m-1}{2m+1}} \exp\left(\frac{hBm}{kT_k}\right)}, \quad (2)$$

where $\alpha = 2^9 \pi^4 / 3hc^3$, μ is the permanent dipole moment of the molecule, B is the molecule's rotational constant, T_r is the radiative temperature, T_k is the kinetic temperature, and C is the averaged collision rate.

Values of $n(J)$ calculated from Equation 2 depend critically on T_r and B , but not as much on T_k , C , and μ within the range of typical values. Thus, as in Oka et al., we set $C = 10^{-7} \text{ s}^{-1}$, $\mu = 4$ Debye, and $T_k = 100 \text{ K}$ [28]; the collision rate is based on a number density of $n \sim 100 \text{ cm}^{-3}$ and collision rate constant $\langle \sigma v \rangle \sim 10^{-9} \text{ cm}^3 \text{ s}^{-1}$, while the kinetic temperature is chosen based on the typical rotational temperatures of 45 K to 200 K for H_2 in interstellar clouds [39]. It is readily shown that $n(J)$ reduces to the Boltzmann distribution with radiative temperature T_r if collisional effects are negligible ($C = 0$), and to that with kinetic temperature T_k if the molecule is non-polar ($\mu = 0$).

The assumed permanent dipole moment of 4 Debye is typical for molecules considered in this paper; see for example Maluendes and McLean [40] for H_2C_n and Woon [41] for HC_n . Varying the dipole moment by factors of a few does not affect the calculation much because of the J^3 factor in the Einstein coefficient A^J .

2.3. Calculating spectral profiles

We use a simplified formula for the energy of spin-orbit interaction and rotation for a $^2\Pi$ electronic state, assuming Hund's case (a) [42]

$$E = A\Sigma\Lambda + BJ(J+1), \quad (3)$$

where A is the spin-orbit splitting constant and Σ ($\pm 1/2$) and Λ (± 1) are the projections of spin angular momentum \mathbf{S} and orbital angular momentum \mathbf{L} , respectively, onto the molecular axis. The spin-orbit interaction splits the ${}^2\Pi$ state into two states with total electron angular momentum $\Omega = \Sigma + \Lambda = (\pm 3/2)$ and $(\pm 1/2)$. These two states are designated as ${}^2\Pi_{3/2}$ and ${}^2\Pi_{1/2}$, with energy $A/2$ and $-A/2$, respectively. Smaller effects such as centrifugal distortion (D), Λ doubling (q), spin-rotation interaction (γ), and hyperfine interaction (a) are neglected. From the energy formula, the line positions are given by:

$$P(J) : \nu = \nu_0 \pm \frac{1}{2}(A' - A) + B'J(J-1) - BJ(J+1) \quad (4a)$$

$$Q(J) : \nu = \nu_0 \pm \frac{1}{2}(A' - A) + (B' - B)J(J+1) \quad (4b)$$

$$R(J) : \nu = \nu_0 \pm \frac{1}{2}(A' - A) + B'(J+1)(J+2) - BJ(J+1), \quad (4c)$$

where ν_0 is the band origin and $+(A' - A)$ and $-(A' - A)$ apply to the ${}^2\Pi_{3/2}$ and ${}^2\Pi_{1/2}$ states, respectively. We denote quantum numbers and molecular constants in the electronic excited states with primes to distinguish from the ground state, which is unprimed.

The relative intensity of a line in an electronic band is given by [43]

$$I \propto \frac{n(J)S}{2J+1}, \quad (5)$$

where S is the appropriate Hönl-London factor, or line strength. For Hund's case (a), the Hönl-London factors are given by [44]

$$P(J) : \frac{J^2 - \Omega^2}{J} \quad (6a)$$

$$Q(J) : \frac{\Omega^2(2J+1)}{J(J+1)} \quad (6b)$$

$$R(J) : \frac{(J+1)^2 - \Omega^2}{J+1}. \quad (6c)$$

Equation 6b indicates that the Q branch line of ${}^2\Pi_{3/2}$ is 9 times stronger than that of ${}^2\Pi_{1/2}$. Therefore, the strong Q branches in Figure 1 indicate that ${}^2\Pi_{3/2}$ and ${}^2\Pi_{1/2}$ are irregular, that is, A is negative [43].

Lines were computed for values of J up to 99, with the assumption that populations in higher levels could be neglected. As J increases, Hund's case (a) gradually shifts to Hund's case (b). However, for the large molecules considered in this paper's simulations, the value of J at which this occurs is so large that the use of Hund's case (a) for the energy and intensity formulae does not introduce serious errors.

Each spectrum is simulated by using the molecular population given in Equation 2, frequencies calculated from Equations 4a-4c, and the corresponding intensity

formulae based on Equations 5 and 6a-6c. Individual lines are broadened by the uncertainty due to the limited time of spontaneous emission and internal conversion [11]. This results in a Lorentzian lineshape with linewidth $\Gamma = \frac{1}{2\pi\Delta t}$, where Δt is the lifetime of the level. Instrumental broadening of the lines was approximated by a Gaussian with a standard deviation of $\sigma = \frac{\nu_0}{2\sqrt{2\ln 2}R}$, where ν_0 is the band origin in Table 1 and R is the instrument resolution. The combination of the effects of lifetime and instrumental broadening results in a Voigt lineshape function.

2.4. Simulating spectra

There are nine variables in the above formalism: the spectroscopic constants $A' - A$, B' , B , the permanent dipole moment in the ground state μ , the radiative and kinetic temperatures T_r and T_k , the average collision rate C , and the line parameters Γ and σ . We use one more variable ρ , the ratio of the peak intensities of the $^2\Pi_{3/2} \leftarrow ^2\Pi_{3/2}$ and the $^2\Pi_{1/2} \leftarrow ^2\Pi_{1/2}$ components, which depends on the populations in each ground state. In principle, this can be calculated from T_r and T_k . However, this would require analyzing the radiative effects of the magnetic dipole moment and magnetic collisions, which are not well known. We therefore leave ρ as a free parameter. σ is held fixed during simulations, since it depends only on the resolving power of the instrument. As noted in the previous section, $n(J)$ is relatively insensitive to changes in T_K , μ , and C ; these parameters were also held fixed. Because the spectrum of $\lambda 5797.1$ toward the star 20 Aql was used as a reference during the simulations, T_r was set to 2.73 K initially. The excitation temperature of CN toward 20 Aql has been measured to be 2.728 K [29], and it is assumed that $T_{ex} = T_r$. Thus, the quantities that were estimated through the modeling process were B , the ratio B'/B , Δt , and the difference in the spin-orbit coupling constants $A' - A$.

Although the spectrum toward ζ Oph in Figure 1 shows the Q -branch most clearly with the high resolution ($R \sim 600,000$) of the AAT, the spectrum is not numerically available. Therefore we use the spectrum toward star 20 Aql reduced by D. E. Welty from data retrieved from the ESO Science Archive Facility (programme IDs 078.C-0403 for the 20 Aql observations by Galazutdinov et al. [34]) as the reference spectrum to compare with our simulation. The High Accuracy Radial Velocity Planet Searcher (HARPS) spectrograph used has lower resolution ($R = 115,000$) and the Q -branch is not as clearly observed, but the spectrum allows for comparisons of the spectral widths between the observed and simulated spectra.

All simulated DIBs were rescaled in the figures to have the same maximum absorption as the given reference spectrum. The absence of Doppler splitting of the interstellar atomic lines toward 20 Aql suggests that the DIB carriers may reside in a single interstellar cloud, which would allow for intrinsic profiles of the $\lambda 5797.1$ band to be observed [34]. Furthermore, since the DIBs toward 20 Aql are among the narrower ones found in published high resolution spectra [26], using 20 Aql for reference facilitates making estimates of a lower bound for B .

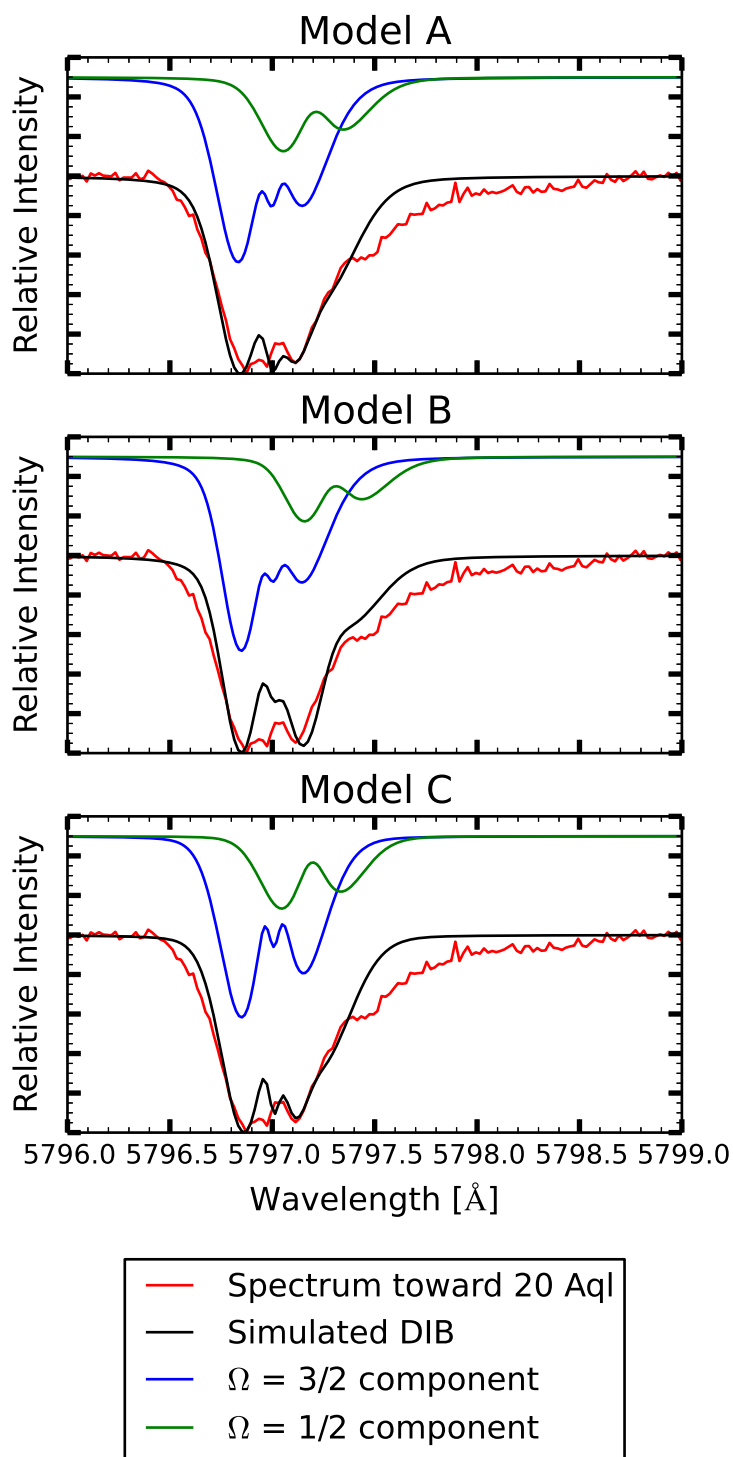


Figure 2. Three examples of simulated spectra for the $\lambda 5797.1$ DIB using a $^2\Pi \leftarrow ^2\Pi$ transition. The observed 20 Aql spectrum (courtesy of D. Welty) is at $R = 115,000$ and based on data obtained from the ESO Science Archive Facility. Models A, B, and C have been calculated using the three sets of parameters listed in Table 1

Table 1. Model input values for the $\lambda 5797.1$ DIB (see fig. 2)

Model	A	B	C
T_r [K]	2.73	2.73	3.50
B [MHz]	1300	1200	1000
B'/B	0.98	0.97	0.99
$A' - A$ [MHz]	19000	27000	17000
λ_0 [\AA]	5797.10	5797.15	5797.10
Δt [ps]	50	50	100
ρ	2.50	3.00	2.50

3. Results

3.1. Modeling the $\lambda 5797.1$ DIB at high resolution

3.1.1. Variation of parameters

The observed $\lambda 5797.1$ DIB toward 20 Aql was simulated by varying parameters. Three examples are shown in Figures 2a, 2b, and 2c, referred to as Models A, B, and C, respectively. The corresponding parameters are given in Table 1. Individual spin-orbit components are drawn above the simulated profile. Out of the 7 parameters shown in Table 1, we found that the 4 parameters T_r , B , $A' - A$ and ρ are crucial in reproducing the spectrum. Though this is too many to fix from a spectrum, we found that they are not tightly correlated. Thus, we could narrow down their values by varying each parameter individually. Model A gives a reasonable agreement, although the shallow bump on the redward side of the DIB is not reproduced. A simulation with larger $A' - A$, as shown in Model B, would shift the $\Omega = 1/2$ spin-orbit component so as to create a small bump on the redward side; however, the central peak then becomes substantially weaker. Increasing T_r could compensate for the narrowing of profiles with smaller values of B , as shown in Model C with $T_r = 3.5$ K. However, as noted earlier, T_r should be close to 2.73 K, the CN excitation temperature for this sightline [29]. Thus, model A is more plausible.

3.1.2. Variation of B

The rotational constant B is the key parameter in simulating the DIB and constraining the size of the carrier molecule. As noted in Section 3.2, B and T_r are two crucial parameters for determining the rotational distribution, but T_r is fixed at 2.73 K. Figure 3 shows the effect of changing B on the profile of the $\lambda 5797.1$ DIB with other parameters fixed at those in Model A. These results show that B is most likely $900 \text{ MHz} < B < 1900 \text{ MHz}$. For a lower B , the full width at half maximum (FWHM) is too small. In addition, the relative strength of the characteristic Q -branch would be too small to be observable because of the high J values required by a smaller B . The line width can be made arbitrarily large by assuming a very small Δt , but then the sharp Q -branch would be washed out. For a larger B , the FWHM is too large and the Q -branch is too strong. The constraints on B indicate that the carrier of the $\lambda 5797$ DIB is a prolate top molecule with 5 to 7 heavy atoms (for comparison, the rotational constant of HC_5N is 1331.3313 MHz [10]).

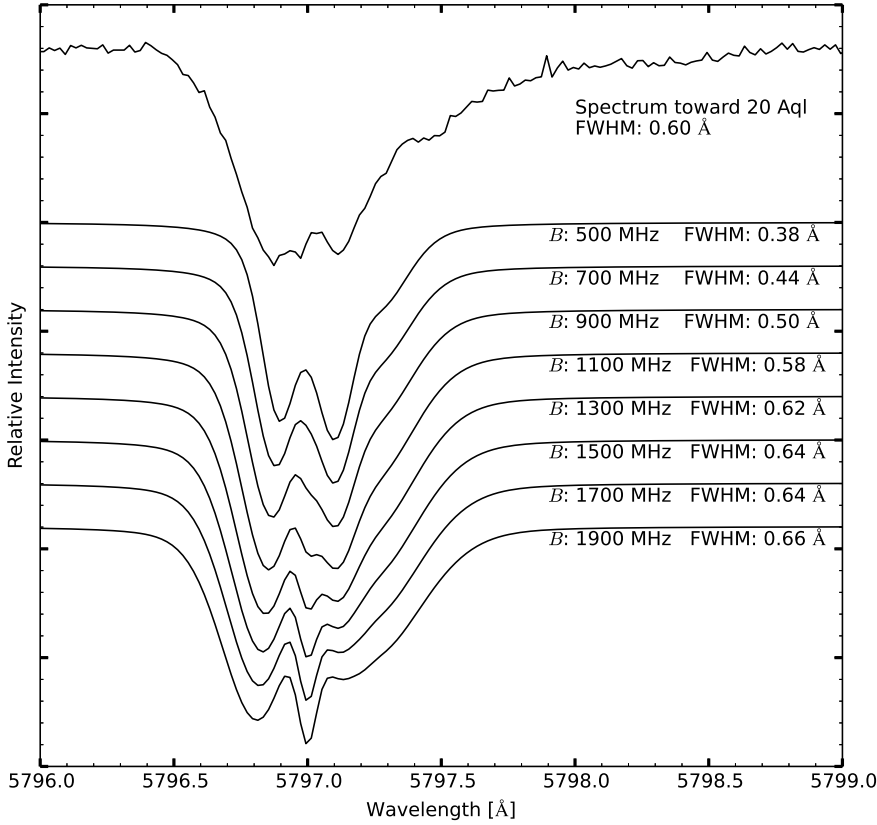


Figure 3. Variation of the simulated spectra as a function of the rotational constant B . The agreement between the simulated and observed full width at half maximum (FWHM) and the visibility of the Q -branch sets the limit of $900 \text{ MHz} \leq B \leq 1900 \text{ MHz}$ which approximately corresponds to $5 \leq n \leq 7$.

4. Discussion

4.1. Constraints on the size of the carrier of the $\lambda 5797.1$ DIB

4.1.1. The present analysis: $5 \leq n \leq 7$

The analysis given above is based on three premises:

- (1) The carrier of the $\lambda 5797.1$ DIB is a polar molecule as concluded by Oka et al. [28]
- (2) The conspicuous central peak in Figure 1 for ζ Oph, ζ Per and μ Sgr of Kerr et al. [33] is a Q -branch of a parallel transition of a prolate top molecule.
- (3) The radiative temperature of the environment is $T_r = 2.73 \text{ K}$.

We believe all of them are valid. We further assumed that the carrier of the DIBs is a linear free radical with a $^2\Pi$ ground state and calculated its parallel band spectrum. A similar formalism may work for a parallel transition of a prolate molecule with rotational constants $A \gg B \sim C$ and with C_{2v} symmetry such as carbenes, H_2C_n , or with $A \gg B$ with C_{3v} symmetry such as methyl-polyynes, $\text{H}_3\text{C}_n\text{H}$. They do not need to be open-shell molecules. In these molecules, the rotational quantum number K_a or K plays the role of Λ of the $^2\Pi$ linear molecules. Prolate tops with C_s symmetry such as CH_2CN^- considered by Cordiner and Sarre [30] cannot produce the Q -branch since the b -type spontaneous emission depopulates the $K_a = 1$ level. Contrary to their argument, rotational levels of ortho and para species are degenerate and they do not keep the $K_a = 1$ level

highly populated.

Although we have only briefly attempted to simulate the $\lambda 5797.1$ DIB using the C_{2v} and C_{3v} prolate tops, we believe that the simulations are similar and that the constraints on B shown in Figure 3 and on n are also applicable for these cases.

In addition to the constraint from this model calculation, two more constraints can be set from other considerations as discussed below.

4.1.2. Upper limit of $n \leq 6$ from the Herschel 36 spectrum

Oka et al. [28] explained the anomalous ETRs observable only toward Herschel 36 as due to a high radiative temperature T_r and a decrease in rotational constants $B' - B$ upon electronic excitation. This decrease is observed in general for most molecules, but the fractional decrease $\beta = (B' - B)/B$ is lower for larger molecules as seen in Table 2 of Ref [28]. Oka et al. set a limit of $|\beta| > 0.015$ assuming $T_r < 100$ K, leading to the constraint $n \leq 6$. This upper limit is not as definitive as that in the previous section in view of the uncertainty of T_r toward Herschel 36. For a higher T_r , the limit $|\beta| > 0.010$ may work, which gives $n \leq 8$ from Table 2 of Ref [28]. However, such a high T_r is not very likely over the long distances through which the DIB molecules are distributed.

4.1.3. Lower limit of $n \geq 5$ from the stability of molecules against photo-dissociation

In dense clouds, gas phase reactions make large molecules from small molecules, as evidenced by the relative abundances of series of molecules. For example, the total column densities of cyano-polyynes $H-(C\equiv C)_n-CN$ for $n = 2 - 4$ toward TMC 1 have been reported to be (in 10^{13} cm^{-2}) 5.0, 1.2, 0.32 by Broten et al. [45], 3.3, 1.1, 0.19 by Bell et al. [46], and 1.1, 1.0, 0.54 by Bell et al. [47]. The values differ due to different treatments of collisions, but we see that the abundance decreases only by a factor of 1 – 4 for each additional $-C\equiv C-$ chain.

The situation is drastically different for diffuse clouds. Oka et al. [48] reported C_2 and C_3 column densities toward 14 stars; their ratios are generally larger than 30 and average to ~ 45 . The high correlation coefficient of 0.93 between them suggests that C_3 is produced by chemical reactions involving C_2 , but the high C_2 to C_3 ratio indicates that photo-dissociation and hydrogenation of C_2 is much faster than the chemical build-up to C_3 . Attempts to detect C_4 and C_5 failed [48, 49]. Molecules detected so far in the optical and infrared regions are all diatomics with the exceptions of H_3^+ and C_3 . Radio observations are more sensitive and have detected triatomics, but H_2CO and the ubiquitous $c-C_3H_2$ and a small amount of $l-C_3H_2$ are the only polyatomics higher than triatomics [50, 51]. All these indicate that abundances of small molecules decrease rapidly with the size of molecules.

On the other hand, the presence of the great many intense DIBs indicates high column densities of large molecules. Using the simple relation between the column density N , equivalent width W_λ , and the transition dipole moment μ_t ,

$$N = \frac{3hcW_\lambda}{8\pi^3\lambda\mu_t^2}, \quad (7)$$

the equivalent widths from 1 to 5700 mÅ of about 400 DIBs observed toward HD 183143 [18] and HD 204827 [17] indicate high column densities on the order of $5 \times 10^{11} \text{ cm}^{-2}$ to $3 \times 10^{15} \text{ cm}^{-2}$ for $\mu_t = 1$ Debye and $5 \times 10^9 \text{ cm}^{-2}$ to $3 \times 10^{13} \text{ cm}^{-2}$ for $\mu_t = 10$ Debye. These are very high column densities and indicate that a large fraction of carbon atoms is locked up in the carriers of DIBs. Moreover, although C_2 and C_3 are undetectable toward the star HD 183143, while they are most abundant

toward the star HD 204827 [48], the two sightlines show comparable intensities for $\lambda 5797.1$ (see Section 4.2.2.) It is highly unlikely that the carriers of DIBs are produced bottom-up from smaller molecules whose column densities are so low. They must be produced top down from the breakdown of dust by cosmic rays or shocks as proposed by Duley [52], most likely from the mixed aromatic/aliphatic organic nanoparticles (MAONS) proposed by Kwok and Zhang [53]. See also Duley et al. [54]. The abundances of the carriers of DIBs must be governed by their stability against photo-dissociation or chemical reactions.

The stability of large carbon molecules C_n has been discussed before in relation to chemical reactions by Freed et al. [55] and Clayton et al. [56]. Their stability argument based on the Rice-Ramsperger-Kassel-Marcus (RRKM) statistical model of unimolecular decomposition can also be applied to stability against photo-dissociation. Namely, the energy of an absorbed photon is distributed among the molecule's great many vibrational states. If infrared photons are emitted before the photon energy is concentrated to break a chemical bond, the molecule survives the photo-excitation. As n gets larger, the number of vibrational modes increases rapidly, and the lifetime of C_n grows. The calculations by Freed et al. [55], summarized in their Figure 1, indicate that the lifetime reaches ~ 1 s at $n = 5$. Since infrared spontaneous emission has a typical lifetime of 30 ms, molecules are stabilized by emitting infrared photons. This sets the lower limit of $n \geq 5$.

4.1.4. $n = 7 - 8$ by Wehres et al.

W. W. Duley drew our attention to Wehres et al. [57], in which they assumed a carbon chain and estimated the number of carbon atom to be 7 to 8. This is for an emission band at 6615 Å from the Red Rectangle whose carrier is perhaps the same as that for $\lambda 6613.6$ DIB. Their estimate is based on the spacing of three satellite lines which they interpret as due to vibrational excitation in the ground state. This is not directly related to the result of our paper but is worthy of notice.

4.2. Further considerations for candidate molecule identification

4.2.1. Candidate molecules in view of Maier laboratory findings

John Maier's laboratory has been extremely prolific in studying electronic optical spectra of unstable species. The number of new spectra discovered in his laboratory in Basel is simply staggering. In the history of molecular spectroscopy involving brilliant scientists, no other group with a professor and collaborators has dominated a field so squarely using so many multifaceted experimental techniques.

One issue with the molecular size constraint discussed in the preceding sections is that many $5 \leq n \leq 7$ molecules as well as larger carbon chain molecules have already been observed in Maier's laboratory and searched for in interstellar space. There are many molecules that have not yet been tested, but one wonders whether such molecules can exist when similar molecular candidates have been rejected. Based on the criteria established by the model, these classes of molecules warrant further investigation as DIB carrier candidates. The following sections discuss the evidence for and against these candidates.

Polar $^2\Pi$ radicals

Radicals HC_n first come to mind as candidates based on the criteria established thus far, but the spectra of HC_5 and HC_7 are perpendicular bands in the wavelength region of interest. They have been observed in the lab and searched for in space [58]. HC_6 has been observed in the laboratory and analyzed in detail; it would seem the most promising both because its parallel band appears in the region of interest and because the sign of the spin-orbit splitting constant is negative ($A = -15.04$ cm $^{-1}$)

[59]. However, a search for it in interstellar space had a negative result [60].

Radical cations $\text{HC}_{n-1}\text{N}^+$ isoelectronic to HC_n are also candidates. Among these, HC_5N^+ has a ${}^2\Pi \leftarrow {}^2\Pi$ band. This molecule has been observed in the laboratory [61] and searched for in interstellar space, also with a negative result [60]. In addition, the cations may not satisfy the stability requirement of Section 4.1.3 because of the rapid dissociative recombination with electrons that is abundant in diffuse clouds.

A series of radicals with a ${}^2\Pi$ ground electronic state whose electronic transitions have not been observed are the HC_{n-1}O molecules observed in the microwave region by the group of Thaddeus and McCarthy [62], the group that has dominated microwave studies of carbon chain molecules. The radicals with $n \leq 4$ are bent in the ground state, but the observed microwave spectra for $n \geq 5$ showed indications of being linear molecules with ${}^2\Pi$ states. The HC_6O radical, which has a negative spin-orbit splitting constant A , is promising. Theoretical calculations have indicated, however, that the Renner-Teller bent ${}^2A''$ state is slightly (320 cm^{-1}) below the ${}^2\Pi$ state [62]. If this is correct, most HC_6O would not be in the ${}^2\Pi$ state because some transition moment must cause the spontaneous emission ${}^2\Pi \rightarrow {}^2A''$. For the isovalent series of molecules HC_{n-1}S , the ground state is ${}^2\Pi$ [63–65].

Radical anions $\text{HC}_{n-1}\text{N}^-$ isoelectronic to HC_{n-1}O radicals are also candidates. Their destruction by C^+ may reduce their abundance, although not to as serious an extent as radical cations destroyed by electrons.

There are other radicals with ${}^2\Pi$ ground states, including ones with Fe, Mg, Si, and S in the chain, but their lower abundances make it less likely that they are carriers of the $\lambda 5797.1$ DIB.

C_{2v} and C_{3v} molecules

Cumulenes, linear H_2C_n , have been observed in the microwave region by Thaddeus’s group in the laboratory for $n = 3 - 9$ [66–69] and in interstellar space for $n = 3$ and 4 [70–72] and 6 [73]. They all have large permanent dipole moments; 4.1, 4.6, 5.9, 6.2 Debye for $n = 3, 4, 5, 6$, respectively [40, 74, 75]. H_2C_n with even n is much more abundant than with odd n . The abundance of H_2C_6 , which is most relevant to discussions in this paper, is reported to be less than that of H_2C_4 by a factor of 25 in TMC-1, but this ratio may well be reversed in diffuse clouds due to the stability against photodissociation discussed in Section 4.1.3. The longest cumulene observed in the optical region is H_2C_3 , which was proposed to be the carrier of the $\lambda 5450$ DIB by Maier et al. [76]. Cumulenes with higher n may well be viable candidates. A recent theoretical paper, however, predicts low oscillator strengths [77] which may make cumulenes unlikely candidates (see Section 4.2.2 below).

The incredibly prolific lab of Thaddeus and McCarthy has produced cumulene derivatives such as $\text{H}_2\text{C}_4\text{N}$, $\text{H}_2\text{C}_6\text{N}$, $\text{H}_2\text{C}_5\text{H}$, $\text{H}_2\text{C}_7\text{H}$ and many C_{3v} molecules [78], all of which could be candidates for the carrier of the $\lambda 5797.1$ DIB if they have electronic transitions in the right wavelength region.

4.2.2. Required high column density

When Maier et al. proposed H_2C_3 as the carrier of the $\lambda\lambda 4881$ and 5450 DIBs, the main objection was that the required H_2C_3 column densities on the order of 5×10^{14} toward HD 183143 and 2×10^{14} toward HD 206267 were far too high [51, 79–81]. Araki et al. [81] searched for the $5_{1,5} \rightarrow 4_{1,4}$ rotational emission at 102.99238 GHz toward HD 183143. Based on the non-detection of the line, they set the upper limit of the H_2C_3 column density to be $1.1 \times 10^{13} \text{ cm}^{-2}$ or $2.0 \times 10^{13} \text{ cm}^{-2}$ for the excitation temperatures of 10 K and 60 K , respectively, assumed by Maier et al. [76]. Their value, however, does not set a valid upper limit. The frequency of 103 GHz ($\sim 4.9 \text{ K}$) is far too high to be radiatively pumped at $T_r = 2.73 \text{ K}$. In addition, the spontaneous emission rate, assuming a permanent

dipole moment of 4.1 Debye [74], would be $9.3 \times 10^{-5} \text{ s}^{-1}$, which is 1000 times higher than the average collision rate of $C = 10^{-7} \text{ s}^{-1}$. The $5_{1,5}$ level won't be populated in diffuse clouds even if the column density of H_2C_3 is high.

Liszt et al. [51] observed the lowest R -branch absorption line $1_{01} \leftarrow 0_{00}$ of para- H_2C_3 at 20792.59 MHz and determined the column density to be on the order of 10^{11} cm^{-2} , three orders of magnitude smaller than that claimed by Maier et al. Although the sightlines observed are not the same as used by Maier et al., approximate proportionality between molecular abundance and the reddening E_{B-V} is used to normalize the column density. The 0_{00} level is certainly populated and this gives the correct column density. A surprising observation in their paper is that the fractional abundances of molecules in Table 4 are similar for diffuse clouds and for TMC-1. If this similarity holds for larger molecules, it will contradict the speculation in Section 5.1.3 of this paper that DIB molecules are produced not by chemical reaction in space but from the breakdown of MAONS. *In order to check this it is important to observe large molecules like H_2C_6 in absorption in the centimeter region.*

In any case, the large column densities required to account for the observed large equivalent widths will present a problem whatever the carrier molecule is. The equivalent width of the $\lambda 5797.1$ DIB has been reported to be 199.0 mÅ toward HD 204827 [17] and 186.4 mÅ toward HD 183143 [18]. From Equation 7, these values correspond to column densities of $8.3 \times 10^{13} \text{ cm}^{-2}$ and $7.7 \times 10^{13} \text{ cm}^{-2}$, respectively, if μ_t is 1 Debye. The column densities are lower by a factor of 100 if μ_t is 10 Debye. The intensity of an electronic transition is often given in terms of the oscillator strength

$$f = \frac{8\pi^2 m_e}{3he^2} \nu \mu_t^2 = 4.701 \times 10^{-7} \tilde{\nu} \tilde{\mu}_t^2 = 8.109 \times 10^{-3} \tilde{\mu}_t^2, \quad (8)$$

where $\tilde{\nu}$ and $\tilde{\mu}_t$ are the frequency of the DIB in cm^{-1} and the transition dipole moment in Debye, respectively, with the last formula applying to the $\lambda 5797.1$ DIB. This indicates that $f = 1$ corresponds approximately to $\tilde{\mu}_t = 10$ Debye. Thus if $f \sim 1$ (e.g. Table 2 of Ref [82]), the required column density is on the order of 10^{12} cm^{-2} , which may be achievable in diffuse clouds.

This paper is dedicated to John P. Maier in appreciation of the inspiration he has given spectroscopists and molecular astrophysicists through his great work over many years. We thank Daniel E. Welty for providing reduced spectra of 20 Aql and Herschel 36 based on data obtained from the ESO Science Archive Facility. We are grateful to M. Araki, W. W. Duley, L. M. Hobbs, M. C. McCarthy, J. P. Maier, P. J. Sarre, P. Sonnentrucker, G. A. H. Walker, D. E. Welty, A. Witt, and D. G. York for reading our draft and giving helpful comments. We also thank two anonymous referees for comments which improved the presentation of this paper. This research was supported by NSF grant 1109014.

References

- [1] G.H. Herbig, Annu. Rev. Astron. Astrophys. **33**, 19 (1995).
- [2] J. Cami and N. Cox, *The Diffuse Interstellar Bands* (Cambridge University Press, Cambridge, 2014).
- [3] A.J. Cannon and E.C. Pickering, The Henry Draper Catalogue **9**, **10**, **11**, 288 (1919).
- [4] A.D. Code, Publ. Astron. Soc. Pac. **70**, 407 (1958).
- [5] G.H. Herbig, Astrophys. J. **196**, 129 (1975).

- [6] M.L. Heger, Lick Obs. Bull. **10**, 146 (1922).
- [7] B.J. McCall and R.E. Griffin, Proc R Soc A **469**, 0604 (2013).
- [8] P.W. Merrill, Publ. Astron. Soc. Pac. **46**, 206 (1934).
- [9] P.W. Merrill and O.C. Wilson, Astrophys. J. **87**, 9 (1938).
- [10] L.W. Avery, N.W. Broten, J.M. MacLeod, T. Oka and H.W. Kroto, Astrophys. J. Lett. **205**, L173 (1976).
- [11] A.E. Douglas, J. Chem. Phys. **45**, 1007 (1966).
- [12] A.E. Douglas, Nature **269**, 130 (1977).
- [13] G.P. van der Zwet and L.J. Allamandola, Astron. Astrophys. **146**, 76 (1985).
- [14] A. Léger and L. d'Hendecourt, Astron. Astrophys. **146**, 81 (1985).
- [15] P.J. Sarre, J. Mol. Spectrosc. **238**, 1 (2006).
- [16] B.A. York, S.L. Ellison, B. Lawton, C.W. Churchill, T.P. Snow, R.A. Johnson and S.G. Ryan, Astrophys. J. Lett. **647**, L29 (2006).
- [17] L.M. Hobbs, D.G. York, T.P. Snow, T. Oka, J.A. Thorburn, M. Bishof, S.D. Friedman, B.J. McCall, B. Rachford, P. Sonnentrucker and D.E. Welty, Astrophys. J. **680**, 1256 (2008).
- [18] L.M. Hobbs, D.G. York, J.A. Thorburn, T.P. Snow, M. Bishof, S.D. Friedman, B.J. McCall, T. Oka, B. Rachford, P. Sonnentrucker and D.E. Welty, Astrophys. J. **705**, 32 (2009).
- [19] A.C. Danks and D.L. Lambert, Mon. Not. R. Astro. Soc. **174**, 571 (1976).
- [20] P.J. Sarre, J.R. Miles, T.H. Kerr, R.E. Hibbins, S.J. Fossey and W.B. Somerville, Mon. Not. R. Astro. Soc. **277**, L41 (1995).
- [21] G.A.H. Walker, A. Webster, D.A. Bohlender and J. Krelowski, Astrophys. J. **561**, 272 (2001).
- [22] P. Ehrenfreund and B.H. Foing, Astron. Astrophys. **307**, L25 (1996).
- [23] T.H. Kerr, R.E. Hibbins, J.R. Miles, S.J. Fossey, W.B. Somerville and P.J. Sarre, Mon. Not. R. Astro. Soc. **283**, L105 (1996).
- [24] S.A. Schulz, J.E. King and R.J. Glinski, Mon. Not. R. Astro. Soc. **312**, 769 (2000).
- [25] J. Cami, F. Salama, J. Jiménez-Vicente, G. Galazutdinov and J. Krelowski, Astrophys. J. **611**, L113 (2004).
- [26] J. Dahlstrom, D.G. York, D.E. Welty, T. Oka, L.M. Hobbs, S. Johnson, S.D. Friedman, Z. Jiang, B.L. Rachford, R. Sherman, T.P. Snow and P. Sonnentrucker, Astrophys. J. **773**, 41 (2013).
- [27] M. Goto, B. Stecklum, H. Linz, M. Feldt, T. Henning, I. Pascucci and T. Usuda, Astrophys. J. **649**, 299 (2006).
- [28] T. Oka, D.E. Welty, S. Johnson, D.G. York, J. Dahlstrom and L.M. Hobbs, Astrophys. J. **773**, 42 (2013).
- [29] A.M. Ritchey, S.R. Federman and D.L. Lambert, Astrophys. J. **728**, 36 (2011).
- [30] M.A. Cordiner and P.J. Sarre, Astron. Astrophys. **472**, 537 (2007).
- [31] C. Cossart-Magos and S. Leach, Astron. Astrophys. **233**, 559 (1990).
- [32] S.A. Edwards and S. Leach, Astron. Astrophys. **272**, 533 (1993).
- [33] T.H. Kerr, R.E. Hibbins, S.J. Fossey, J.R. Miles and P.J. Sarre, Astrophys. J. **495**, 941 (1998).
- [34] G.A. Galazutdinov, G. Lo Curto and J. Krelowski, Mon. Not. R. Astro. Soc. **386**, 2003 (2008).
- [35] G.A. Galazutdinov, G. Lo Curto and J. Krelowski, Astrophys. J. **682**, 1076 (2008).
- [36] S.D. Friedman, D.G. York, B.J. McCall, J. Dahlstrom, P. Sonnentrucker, D.E. Welty, M.M. Drosback, L.M. Hobbs, B.L. Rachford and T.P. Snow, Astrophys. J. **727**, 33 (2011).
- [37] W.W. Duley and S. Kuzmin, Astrophys. J. Lett. **712**, L165 (2010).
- [38] T. Oka, D.E. Welty, S. Johnson, D.G. York, J. Dahlstrom and L.M. Hobbs, Astrophys. J. **793**, 68 (2014).
- [39] E.F. van Dishoeck and J.H. Black, Astrophys. J. Suppl. Ser. **62**, 109 (1986).
- [40] S.A. Maluendes and A.D. McLean, Chem. Phys. Lett. **200**, 511 (1992).
- [41] D.E. Woon, Chem. Phys. Lett. **244**, 45 (1995).
- [42] L.D. Landau and E.M. Lifshitz, *Quantum Mechanics: Non-Relativistic Theory*, 3rd ed. (Pergamon Press, New York, 1977).
- [43] G. Herzberg, *Molecular Spectra and Molecular Structure I. Spectra of Diatomic Molecules*, 2nd ed. (Krieger Publishing Company, Malabar, Florida, 1989).
- [44] I. Kovács, *Rotational Structure in the Spectra of Diatomic Molecules*, 1st ed. (Akademiai Kiado, Budapest, 1969).
- [45] N.W. Broten, T. Oka, L.W. Avery, J.M. MacLeod and H.W. Kroto, Astrophys. J. Lett. **223**, L105 (1978).
- [46] M.B. Bell, P.A. Feldman, M.J. Travers, M.C. McCarthy, C.A. Gottlieb and P. Thaddeus, Astrophys. J. Lett. **483**, L61 (1997).
- [47] M.B. Bell, J.K.G. Watson, P.A. Feldman and M.J. Travers, Astrophys. J. **508**, 286 (1998).

- [48] T. Oka, J.A. Thorburn, B.J. McCall, S.D. Friedman, L.M. Hobbs, P. Sonnentrucker, D.E. Welty and D.G. York, *Astrophys. J.* **582**, 823 (2003).
- [49] J.P. Maier, G.A.H. Walker and D.A. Bohlender, *Astrophys. J.* **566**, 332 (2002).
- [50] T.P. Snow and B.J. McCall, *Annu. Rev. Astron. Astrophys.* **44**, 367 (2006).
- [51] H. Liszt, P. Sonnentrucker, M. Cordiner and M. Gerin, *Astrophys. J. Lett.* **753**, L28 (2012).
- [52] W.W. Duley, *Faraday Discuss.* **133**, 415 (2006).
- [53] S. Kwok and Y. Zhang, *Astrophys. J.* **771**, 5 (2013).
- [54] W.W. Duley, A. Zaidi, M.J. Weslowski and S. Kuzmin, *Mon. Not. R. Astro. Soc.* **447**, 1242 (2015).
- [55] K.F. Freed, T. Oka and H. Suzuki, *Astrophys. J.* **263**, 718 (1982).
- [56] D.D. Clayton, W. Liu and A. Dalgarno, *Science* **283**, 1290 (1999).
- [57] N. Wehres, H. Linnartz, H. van Winckel and A.G.G.M. Tielens, *Astron. Astrophys.* **533**, A28 (2011).
- [58] H. Ding, T. Pino, F. Güthe and J.P. Maier, *J. Chem. Phys.* **117**, 8362 (2002).
- [59] H. Linnartz, T. Motylewski, O. Vaizert, J.P. Maier, A.J. Apponi, M.C. McCarthy, C.A. Gottlieb and P. Thaddeus, *J. Mol. Spectrosc.* **197**, 1 (1999).
- [60] T. Motylewski, H. Linnartz, O. Vaizert, J.P. Maier, G.A. Galazutdinov, F.A. Musaev, J. Krelowski, G.A.H. Walker and D.A. Bohlender, *Astrophys. J.* **531**, 312 (2000).
- [61] W.E. Sinclair, D. Pfluger and J.P. Maier, *J. Chem. Phys.* **111**, 9600 (1999).
- [62] S. Mohamed, M.C. McCarthy, A.L. Cooksy, C. Hinton and P. Thaddeus, *J. Chem. Phys.* **123**, 234301 (2005).
- [63] M. Nakajima, Y. Sumiyoshi and Y. Endo, *Chem. Phys. Lett.* **355**, 116 (2002).
- [64] A. Denisov, T.W. Schmidt, A.E. Boguslavskiy, H. Ding, M. Araki and J.P. Maier, *Int. J. Mass Spectrom.* **233**, 131 (2004).
- [65] A. Mitrushchenkov, R. Linguerr, P. Rosmus and J.P. Maier, *Mol. Phys.* **107**, 1549 (2009).
- [66] J.M. Vrtilek, A. Gottlieb, E.W. Gottlieb, T.C. Killian and P. Thaddeus, *Astrophys. J. Lett.* **364**, L53 (1990).
- [67] T.C. Killian, J.M. Vrtilek, C.A. Gottlieb, E.W. Gottlieb and P. Thaddeus, *Astrophys. J. Lett.* **365**, L89 (1990).
- [68] M.C. McCarthy, M.J. Travers, A. Kovacs, W. Chen, S.E. Novick, C.A. Gottlieb and P. Thaddeus, *Science* **275**, 518 (1997).
- [69] A.J. Apponi, M.C. McCarthy, C.A. Gottlieb and P. Thaddeus, *Astrophys. J.* **530**, 357 (2000).
- [70] J. Cernicharo, C.A. Gottlieb, M. Guelin, T.C. Killian, G. Paubert, P. Thaddeus and J.M. Vrtilek, *Astrophys. J. Lett.* **368**, L39 (1991).
- [71] J. Cernicharo, C.A. Gottlieb, M. Guelin, T.C. Killian, P. Thaddeus and J.M. Vrtilek, *Astrophys. J. Lett.* **368**, L43 (1991).
- [72] K. Kawaguchi, N. Kaifu, M. Ohishi, S.I. Ishikawa, Y. Hirahara, S. Yamamoto, S. Saito, S. Takano, A. Murakami, J.M. Vrtilek, C.A. Gottlieb, P. Thaddeus and W.M. Irvine, *Publ. Astron. Soc. Japan* **43**, 607 (1991).
- [73] W.D. Langer, T. Velusamy, T.B.H. Kuiper, R. Peng, M.C. McCarthy, M.J. Travers, A. Kovács, C.A. Gottlieb and P. Thaddeus, *Astrophys. J. Lett.* **480**, L63 (1997).
- [74] D.J. Defrees and A.D. McLean, *Astrophys. J. Lett.* **308**, L31 (1986).
- [75] C.E. Dykstra, C.A. Parsons and C.L. Oates, *J. Am. Chem. Soc.* **101**, 1962 (1979).
- [76] J.P. Maier, G.A.H. Walker, D.A. Bohlender, F.J. Mazzotti, R. Raghunandan, J. Fulara, I. Garkusha and A. Nagy, *Astrophys. J.* **726**, 41 (2011).
- [77] Y. Zhang, L. Wang, Y. Li and J. Zhang, *J. Chem. Phys.* **138**, 204303 (2013).
- [78] P. Thaddeus and M.C. McCarthy, *Spectrochim. Acta A* **57**, 757 (2001).
- [79] T. Oka and B.J. McCall, *Science* **331**, 293 (2011).
- [80] J. Krelowski, G. Galazutdinov and R. Kołos, *Astrophys. J.* **735**, 124 (2011).
- [81] M. Araki, S. Takano, H. Yamabe, K. Tsukiyama and N. Kuze, *Astrophys. J. Lett.* **753**, L11 (2012).
- [82] S.M.E. Joseph, J. Fulara, I. Garkusha and J.P. Maier, *Mol. Phys.* **111**, 1977 (2013).

Appendix A. Re-examination of the Anomalous Her 36 DIBs

Our use of the $^2\Pi \leftarrow ^2\Pi$ parallel band for the $\lambda 5797.1$ DIB in this paper contradicts the use of the $^2\Pi \leftarrow ^2\Sigma$ perpendicular band by Oka et al. [28] to account for the ETR toward the star Herschel 36. The perpendicular band was used since a parallel band cannot simulate the ETR if a uniform high radiative temperature T_r is assumed.

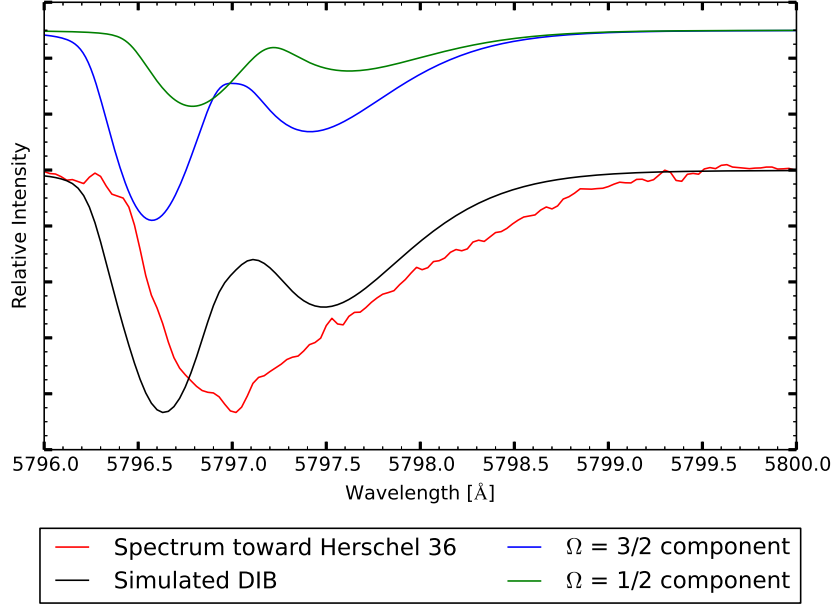


Figure A1. Simulation of the anomalous $\lambda 5797.1$ DIB toward Her 36 using a $^2\Pi \leftarrow ^2\Pi$ parallel transition, $T_r = 25$ K, $\lambda_0 = 5797.25$ Å. All other model input values equal to those of Model A. The parallel band based on a single T_r does not reproduce the observed spectrum. The $R = 48000$ Her 36 spectrum (courtesy of Dan Welty) was retrieved from the ESO Science Archive Facility.

An example of a simulation of the $\lambda 5797.1$ DIB as a parallel band using $T_r = 25$ K, $\lambda_0 = 5797.25$ Å, and the remaining parameters fixed at the values in Model A of this paper is presented in Fig. A1. The two distinct peaks differ from the observed single peak and this dilemma cannot be fixed as long as we use a single T_r .

In actuality, T_r varies along the line of sight from very high T_r near Her 36 SE to $T_r = 2.73$ K at greater distances from this infrared source. The value of T_r used by Oka et al. [28] is an effective temperature after a very complicated average. Since taking into account the variation of T_r along the line of sight is a difficult task, here we add spectra calculated with $T_r = 30$ K and $T_r = 2.73$ K. Fig. A2 provides an example. The ETR is reproduced by the band at the higher temperature, and the double-peaked structure of the parallel band at the higher temperature is “filled in” by the transition occurring at a lower temperature. Thus the ETR on $\lambda 5797.1$ DIB can be reproduced by a perpendicular band as well as by a parallel band as long as the fraction of the variation of the B rotational constant β is sufficiently high.

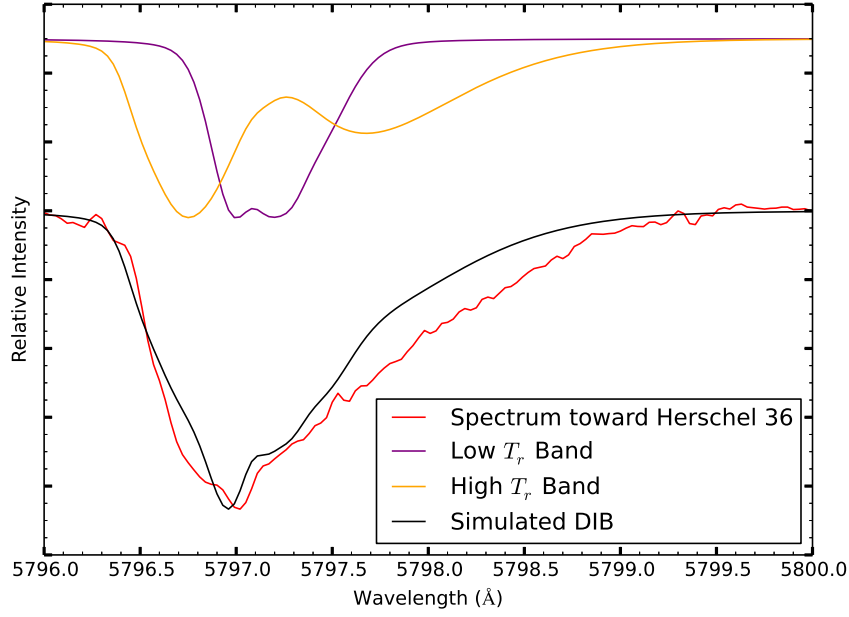


Figure A2. Alternative simulation of the anomalous $\lambda 5797.1$ DIB toward Her 36 using the parallel $^2\Pi \leftarrow ^2\Pi$ transition using two radiative temperatures $T_r = 2.73$ K for narrow component and $T_r = 30$ K for the broader component. See appendix for further explanation.